International Journal of Solids and Structures 50 (2013) 2970–2979

Contents lists available at SciVerse ScienceDirect

International Journal of Solids and Structures

journal homepage: www.elsevier.com/locate/ijsolstr

Nonlinear dynamic model with multi-fields coupling effects for giant magnetostrictive actuators

Tian-Zhong Wang [a,b,c], You-He Zhou [b,c,*]

[a] Institute of Systems Engineering, China Academy of Engineering Physics, Mianyang 621900, People's Republic of China
[b] Key Laboratory of Mechanics on Disaster and Environment in Western China, Lanzhou University, Ministry of Education, Lanzhou 730000, People's Republic of China
[c] Department of Mechanics and Engineering Science, College of Civil Engineering and Mechanics, Lanzhou University, Lanzhou 730000, People's Republic of China

ARTICLE INFO

Article history:
Received 14 December 2012
Received in revised form 1 May 2013
Available online 23 May 2013

Keywords:
Terfenol-D
Magnetostriction
Nonlinearity
Multi-fields coupling
Frequency-dependent hysteresis

ABSTRACT

This paper addresses the modeling of complex hysteresis behavior for giant magnetostrictive actuator system under magnetically unbiased conditions. The hysteresis behavior is modeled by establishing a novel nonlinear dynamic model with multi-fields coupling effects, in which both the eddy current effects and the change of stress are considered. The former is included in the nonlinear transient constitutive model with magnetic-elastic-thermal coupling effect, which is employed as the basic constitutive equations of Terfenol-D. The latter is characterized through the structural dynamic behavior of actuator system itself, which is modeled by theorem of momentum. The quantitative agreements between numerical simulation results and existing experimental data indicate that nonlinear dynamic model can accurately describe the complex hysteresis behavior of the giant magnetostrictive actuator system not only under quasi-static operating conditions but also under dynamic operating conditions. The numerical simulation results also indicate that both the eddy current effects and structural dynamic behavior are the origin of frequency-dependent hysteresis behavior for giant magnetostrictive actuator system, and demonstrate the significance and necessity of simultaneously considering the eddy current effects and the change of stress in the system-level. Thus, the nonlinear dynamic model established in this paper is a system-lever coupled theoretical model, which can be directly used in the active vibration control and any other engineering application of the giant magnetostrictive actuators.

1. Introduction

Magnetostriction is the phenomenon of strong coupling between magnetic state and mechanical state of magnetostrictive materials: strains are generated in response to an applied magnetic field, whereas mechanical stresses in the materials produce measurable changes in magnetization. As a kind of typical magnetostrictive materials, Terfenol-D has some distinct advantages over other smart materials, such as large strain, high force, fast response, simple driving, high energy coupling factor, wide frequency rang and so on (Grunwald and Olabi, 2008; Olabi and Grunwald, 2008; Pradhan, 2005; Shang et al., 2008; Sun and Zheng, 2006; Valadkhan et al., 2010; Zheng et al., 2007; Zhou et al., 2006). In such a case, Terfenol-D has immeasurable applied prospect in ultrasonic transducers, active vibration absorbers, robotics, linear motors, micropumps, microvalves, micropositioners, etc, especially in high performance actuator and sensor systems (Grunwald and Olabi, 2008; Olabi and Grunwald, 2008; Shang et al., 2008; Sun and Zheng, 2006), which are being increasingly used in industrial, biomedical and defense fields (Grunwald and Olabi, 2008; Olabi and Grunwald, 2008; Pradhan, 2005).

However, like piezoelectric materials and shape memory alloy, many experiments have shown that the magnetostrictive effect of Terfenol-D exhibits frequency-dependent hysteresis and magnetic-elastic-thermal coupling nonlinear constitutive behavior (Bottauscio et al., 2008; Calkins et al., 1997; Clark et al., 1988; Faidley et al., 1998; Gao et al., 2008; Liang and Zheng, 2007; Lovisolo et al., 2008; Mahadevan et al., 2010; Moffett et al. 1991; Slaughter et al., 2000; Smith et al., 2006), which is named material coupling in this paper Hirsinger and Billardon (1995). When an alternating magnetic field is applied in the giant magnetostrictive actuator system depicted in Fig. 1, then the active element in the actuator system (i.e., Terfenol-D rod) produces length variation following the input magnetic field and transfers the electromagnetic energy into the structural vibration based on the direct magnetostrictive effect. Meanwhile, the structural vibration of the actuator system also causes the mechanical state variation and ensuing magnetic state variation in the Terfenol-D rod due to the converse

* Corresponding author at: Key Laboratory of Mechanics on Disaster and Environment in Western China, Lanzhou University, Ministry of Education, Lanzhou 730000, People's Republic of China. Tel.: +86 0931 8910340; fax: +86 0931 8625576.
E-mail addresses: wangtianzh09@lzu.edu.cn (T.-Z. Wang), zhouyh@lzu.edu.cn (Y.-H. Zhou).

0020-7683/$ - see front matter © 2013 Elsevier Ltd. All rights reserved.
http://dx.doi.org/10.1016/j.ijsolstr.2013.05.012

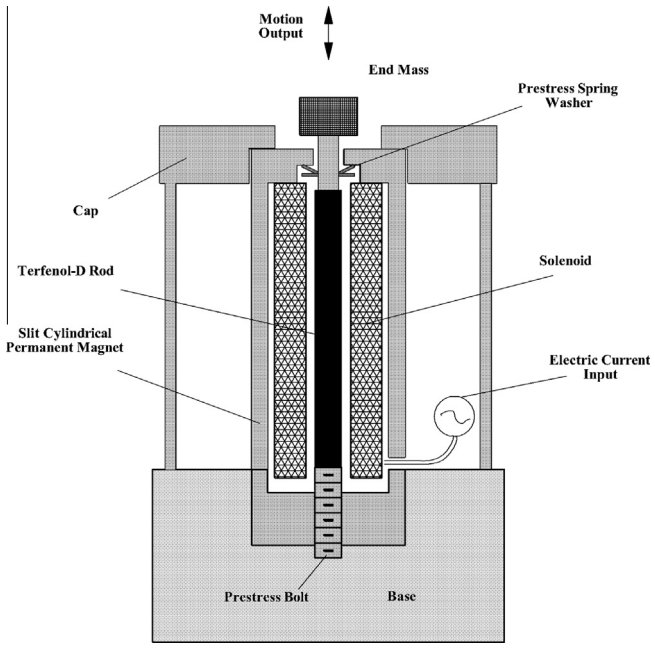

Fig. 1. Schematic of a prototypical giant magnetostrictive actuator.

magnetostrictive effect. For the giant magnetostrictive actuator system, in other words, there is strong coupling interaction between the nonlinear constitutive behavior of Terfenol-D and the structural dynamic behavior of the actuator system itself. It is so-called structural coupling in the references Hirsinger and Billardon (1995), which motivates consideration of the actuator system as a whole. These two kinds of strong coupling interaction mentioned above must severely limit the giant magnetostrictive actuator system's performances such as undesirable position error, oscillation, or instability, and hinder its further application in active vibration control (Johnson et al., 1992; Tan and Baras, 2004). Therefore, from both the fundamental perspective of the actuator accurate characterization and the practical perspective of subsequent model-based active vibration control development, it is quite significant and necessary to establish a system-lever coupled theoretical model simultaneously incorporating the material coupling and structural coupling for the giant magnetostrictive actuator system.

For the complex nonlinear constitutive behavior of Terfenol-D measured in the experiments, numerous nonlinear models have been established including the Jiles-Atherton model (Jiles and Atherton, 1986), Armstrong model (Armstrong, 1997), Preisach model (Reimers and Torre, 1999) and dynamic actuation models in which eddy current losses have been modeled as a one-dimensional magnetic diffusion problem in cylindrical coordinates (Chakrabarti and Dapino, 2010; Sarawate and Dapino, 2008), as well as the more recent dynamic hysteresis constitutive model (Zheng et al., 2009), energy-averaged model (Chakrabarti and Dapino, 2012a), dynamic loss hysteresis model (Xu et al., 2013), nonlinear transient constitutive model (Wang and Zhou, 2010), etc. Among these models, the nonlinear transient constitutive model established by Wang and Zhou (2010) , which is based on the thermodynamic theory and the energy balance principle, can simultaneously and accurately describe frequency-dependent hysteresis and magnetic-elastic-thermal coupling nonlinear constitutive behavior inherent to Terfenol-D under various mechanical and magnetic loading conditions as well as working temperature, including the temperature-dependent saturation nonlinearity and "overturn phenomenon" with hysteresis (Wang and Zhou, 2011, 2010). That is to say, the first kind of coupling issue involved in the giant magnetostrictive actuator system is perfectly solved by the nonlinear transient constitutive model. However, it is purely material constitutive model and does not incorporate the structural dynamic behavior arising from the actuator operation. Thus, it does not refer to the second kind of coupling issue involved in the giant magnetostrictive actuator system. For the system-level structural dynamic behavior of the magnetostrictive smart structures, both the discrete finite element models (Chakrabarti and Dapino, 2012b; Evans and Dapino, 2011; Graham et al., 2009; Kannan and Dasgupta, 1997; Pérez-Aparicio and Sosa, 2004; Slaughter, 2009) and the lumped parameter models (Dapino et al., 2002, 2000a,b; Nealis and Smith, 2007; Slaughter et al., 2000) have been developed. Here, it should be noted that Dapino and Smith et al. have done many works to develop theoretical models that can describe the structural dynamic behavior for Terfenol-D based actuators (Dapino et al., 2002, 2000a,b; Nealis and Smith, 2007; Slaughter et al., 2000). Since the material coupling issue inherent to Terfenol-D was not perfectly solved at that time, the complexly nonlinear multi-fields coupling behavior of Terfenol-D measured in the experiments is not sufficiently taken into account in these theoretical models, especially for the temperature effect. Moreover, most of these theoretical models can only be used to simulate the operating conditions of quasi-static state or low frequency exciting and cannot capture the frequency-dependent hysteresis behavior at high frequency exciting for the magnetostrictive actuator systems due to unconsidered eddy current effects (Dapino et al., 2002, 2000a,b; Nealis and Smith, 2007).

In this paper, we mainly focus on the complex hysteresis behavior of the giant magnetostrictive actuator system under magnetically unbiased conditions. Based on the nonlinear transient constitutive model with eddy current effects of Terfenol-D proposed previously by the author of this paper (Wang and Zhou, 2010), a nonlinear dynamic model with multi-fields coupling effects is established in Section 2 for the giant magnetostrictive actuator system, in which strong coupling interaction between the nonlinear constitutive behavior of Terfenol-D and the structural dynamic behavior of the actuator system itself is accounted for through theorem of momentum. For quantitative purposes, an appropriate numerical approximation method for solving the strongly nonlinear multi-fields coupling problem is proposed in Section 3. After that, the validity and reliability of the obtained nonlinear dynamic model and its approximation method are verified in Section 4 by comparing its quantitative predictions with those existing experimental data, wherein the influences of the eddy current effects and the structural dynamic behavior on the hysteresis behavior of the giant magnetostrictive actuator system are also investigated in detail. Finally, some conclusions are summarized in Section 5.

2. Theoretical framework

In this section, we briefly display the derivation process of the nonlinear dynamic model with multi-fields coupling effects for the giant magnetostrictive actuator system depicted in Fig. 1, in which the Terfenol-D rod is the active element. As detailed in the references Al-Jiboory and Lord (1990), Shang et al. (2008), Zhou et al. (2006), it is a typical giant magnetostrictive actuator currently employed in many structural applications, and illustrates the various physical components that must be modeled to fully utilize the giant magnetostrictive actuator capabilities. Thus, it provides a template for the development of models which will ultimately enhance design and performance. The primary components of the giant magnetostrictive actuators are a cylindrical Terfenol-D rod, a solenoid, an enclosing slit cylindrical permanent magnet, a prestress bolt and a prestress spring washer. The prestress bolt and spring washer allows the Terfenol-D rod to be

placed under a variable mechanically compressive stress state, which increases the distribution of magnetic moments perpendicular to the rod axis. Application of current to the solenoid then produces a magnetic field that causes movement of domain wall and rotation of magnetic moments within the Terfenol-D rod. The resulting strains or forces provide the actuator capabilities for the actuator. The capability for attaining bidirectional strains or forces is provided by a dc magnetic bias field generated by the enclosing cylindrical permanent magnet (alternatively, a biasing dc current could be applied to the solenoid).

For modeling purposes, the cylindrical Terfenol-D rod in the giant magnetostrictive actuator system can be looked as a fixed-free elastic rod without loss of generality, which has length l and diameter D. Assume that the longitudinal coordinate spans from the fixed end ($x = 0$). Let $u(x, t)$ and $\varepsilon(x, t)$ be the longitudinal displacement and total strain of the rod at position x and time t relative to the unstressed state. Then we can get the following geometrical equation:

$$\varepsilon(x,t)=\frac{\partial u(x,t)}{\partial x} \tag{1}$$

As indicated in the introduction and elsewhere (Wang and Zhou, 2010), there are two kinds of strongly nonlinear multi-fields coupling problem in the giant magnetostrictive actuator system, and the first kind of coupling problem (i.e., material coupling) has already been perfectly solved by the nonlinear transient constitutive model with eddy current effects proposed previously by the author of this paper. In this case, the nonlinear transient constitutive model with eddy current effects (Wang and Zhou, 2010) is employed as the basic constitutive equations of the Terfenol-D rod, which can be written as

$$\varepsilon(x,t)=\frac{\sigma(x,t)}{E_S}+\alpha[T(x,t)-T_r]-\frac{\tilde{B}}{M_S^2}[T(x,t)-T_r]M(x,t)^2 + \begin{cases} \lambda_S\tanh\left(\frac{\sigma(x,t)}{\sigma_S}\right)+\frac{\left[1-\tanh\left(\frac{\sigma(x,t)}{\sigma_S}\right)\right]\lambda_S}{M_S^2}M(x,t)^2 & \left(\frac{\sigma(x,t)}{\sigma_S}\geqslant 0\right) \\ \frac{\lambda_S}{2}\tanh\left(\frac{2\sigma(x,t)}{\sigma_S}\right)+\frac{\left[2-\tanh\left(\frac{2\sigma(x,t)}{\sigma_S}\right)\right]\lambda_S}{2M_S^2}M(x,t)^2 & \left(\frac{\sigma(x,t)}{\sigma_S}<0\right) \end{cases} \tag{2}$$

$$\mu_0\delta_M\frac{D^2}{2\theta\beta}\left(\frac{\partial M(x,t)}{\partial t}\right)^2+\mu_0^{\frac{1}{2}}\delta_M\left(\frac{G_0S_0H_0}{\theta}\right)^{\frac{1}{2}}\left(\frac{\partial M(x,t)}{\partial t}\right)^{\frac{3}{2}} +\left\{\varsigma K-\delta_M\bar{\eta}(x,t)[M_{an}(x,t)-M(x,t)]-c\varsigma K\bar{\eta}(x,t)\frac{dM_{an}(x,t)}{dH_{eff}(x,t)}\right\}\frac{\partial M(x,t)}{\partial t} -\left\{\delta_M[M_{an}(x,t)-M(x,t)]+c\varsigma K\frac{dM_{an}(x,t)}{dH_{eff}(x,t)}\right\}\frac{dH(t)}{dt}=0 \tag{3}$$

in which the anhysteretic magnetization $M_{an}(x, t)$ and the effective magnetic field $H_{eff}(x, t)$ as well as the assistant variable $\bar{\eta}(x, t)$ can be respectively formulated as follows (Wang and Zhou, 2010):

$$M_{an}(x,t)=M_S\frac{[T_C-T(x,t)]^{0.5}}{(T_C-T_r)^{0.5}} \times\left[\coth\left(\frac{3\chi_m(T_C-T_r)^{0.5}}{M_S[T_C-T(x,t)]^{0.5}}\right)H_{eff}(x,t)-\frac{M_S[T_C-T(x,t)]^{0.5}}{3\chi_m(T_C-T_r)^{0.5}H_{eff}(x,t)}\right] \tag{4}$$

$$H_{eff}(x,t)=H(t)+\eta M(x,t)-\frac{3\tilde{B}\sigma(x,t)M(x,t)[T(x,t)-T_r]}{\mu_0M_S^2} +\begin{cases} \frac{3\left[1-\tanh\left(\frac{\sigma(x,t)}{\sigma_S}\right)\right]\lambda_S}{\mu_0M_S^2}\sigma(x,t)M(x,t) & \left(\frac{\sigma(x,t)}{\sigma_S}\geqslant 0\right) \\ \frac{3\left[2-\tanh\left(\frac{2\sigma(x,t)}{\sigma_S}\right)\right]\lambda_S}{2\mu_0M_S^2}\sigma(x,t)M(x,t) & \left(\frac{\sigma(x,t)}{\sigma_S}<0\right) \end{cases} \tag{5}$$

$$\bar{\eta}(x,t)=\eta-\frac{3\tilde{B}\sigma(x,t)[T(x,t)-T_r]}{\mu_0M_S^2} +\begin{cases} \frac{3\left[1-\tanh\left(\frac{\sigma(x,t)}{\sigma_S}\right)\right]\lambda_S\sigma(x,t)}{\mu_0M_S^2} & \left(\frac{\sigma(x,t)}{\sigma_S}\geqslant 0\right) \\ \frac{3\left[2-\tanh\left(\frac{2\sigma(x,t)}{\sigma_S}\right)\right]\lambda_S\sigma(x,t)}{2\mu_0M_S^2} & \left(\frac{\sigma(x,t)}{\sigma_S}<0\right) \end{cases} \tag{6}$$

In Eqs. (2)–(6), the variables $\sigma(x, t)$, $T(x, t)$, $H(t)$ and $M(x, t)$ denote, respectively, the true stress, the temperature, the applied magnetic field and the corresponding magnetization. The material parameters appearing in Eqs.)(2)–(6) concretely include α, T_r, $\tilde{B}$, M_S, λ_S, σ_S, E_S, μ_0, δ_M, θ, β, G_0, S_0, H_0, ζ, K, c, η, T_C and χ_m, which have definitely physical implications and can be determined by the present physical or material experiments. For instance, $\mu_0 = 4\pi \times 10^{-7}$ H/m is the vacuum permeability, E_S is the intrinsic Young's modulus at the saturation segment, α is the constant of thermal expansion, T_r is the spin reorientation temperature with $T_r = 0$ °C for Terfenol-D (Al-Jiboory and Lord, 1990), T_c is the Curie temperature with $T_c = 383.3$ °C for Terfenol-D (Dhilsha and Rama Rao, 1993), M_S is a saturation magnetization when $T(x, t) = T_r$, λ_S is the saturation magnetostrictive coefficient when $\sigma(x, t) = 0$ and $T(x, t) = T_r$, θ is the resistivity with dimension of Ω m, β is a geometrical factor with $\beta = 16$ for cylinders (Jiles, 1994), G_0 is a dimensionless constant with value $G_0 = 0.1356$ (Jiles, 1994), $S_0 = \pi\left(\frac{D}{2}\right)^2$ is the cross-sectional area of the cylindrical Terfenol-D rod, H_0 is the internal potential experienced by domain walls with dimension of Am^{-1}, χ_m is the magnetic susceptibility in the initial linear region, c is a reversibility coefficient and can be estimated from the ratio of the initial and anhysteretic differential susceptibilities. The non-negative constant K is a micro-structural parameter with dimension of Am^{-1}, which is proportional to the pinning sites density and pinning sites energy, and provides a measure for the average energy required to break a pinning site. The dimensionless parameter η is the Weiss molecular field coefficient, which is used to quantify the amount of interaction between neighbouring magnetic moments. The parameter $\tilde{B}$ is the slope determined by the saturation magnetostrictive strain-temperature curve, which is a constant independent on the temperature due to the linear dependence of the saturation magnetostrictive strain on the temperature for Terfenol-D (Clark and Crowder, 1985). The reference stress $\sigma_S = \frac{\lambda_S E_S E_0}{(E_S - E_0)}$, in which E_0 is the initial Young's modulus. The parameter ζ takes the value +1 when the applied magnetic field $H(t)$ increases and -1 when the applied magnetic field $H(t)$ decreases to ensure that the pinning sites always oppose changes in magnetization. The parameter δ_M is used to guarantee that the calculation results are coincident with the physical properties of Terfenol-D, which can be expressed as follows (Iyer and Krishnaprasad, 2005):

$$\delta_M=\begin{cases} 0: \frac{dH(t)}{dt}<0 \text{ and } M_{an}(x,t)-M(x,t)>0, \\ 0: \frac{dH(t)}{dt}>0 \text{ and } M_{an}(x,t)-M(x,t)<0, \\ 1: \text{otherwise}. \end{cases} \tag{7}$$

Now, let us qualitatively evaluate main features of the nonlinear transient constitutive model expressed by Eqs. (2) and (3). Firstly, from the expression of the effective magnetic field $H_{eff}(x, t)$ (i.e., Eq. (5)), one can find that besides the applied magnetic field (i.e., $H(t)$) and Weiss molecular field (i.e., $\eta M(x, t)$), the effective magnetic field H_{eff} also includes the contribution of field relate to magnetic-elastic interactions (i.e., $\frac{3\left[1-\tanh\left(\frac{\sigma(x,t)}{\sigma_S}\right)\right]\lambda_S}{\mu_0M_S^2}\sigma(x,t)M(x,t)$ when $\frac{\sigma(x,t)}{\sigma_S}\geqslant 0$, or $\frac{3\left[2-\tanh\left(\frac{2\sigma(x,t)}{\sigma_S}\right)\right]\lambda_S}{2\mu_0M_S^2}\sigma(x,t)M(x,t)$ when $\frac{\sigma(x,t)}{\sigma_S}<0$) as well as the contribution of field relate to magnetic-elastic-thermal

interactions (i.e., $-\frac{3\tilde{B}\sigma(x,t)M(x,t)[T(x,t)-T_r]}{\mu_0 M_S^2}$). Thus, the effects of the dynamic stress $\sigma(x, t)$ and temperature $T(x, t)$ on the effective magnetic field $H_{eff}(x, t)$ and ensuing magnetization $M(x, t)$ are incorporated in the nonlinear transient constitutive model. Secondly, the first and second terms in Eq. (3) represent the classical eddy current loss and anomalous loss, respectively. In such a case, the nonlinear transient constitutive model is applicable not only for low frequency quasi-static operating conditions but also for high frequency dynamic operating conditions. Finally, it should be noted that Eq. (2) is nonlinear and magnetic-elastic-thermal coupling. The terms in the right hand side of Eq. (2) can be divided into four kinds. The first consists of the terms dependent only the stress $\sigma(x, t)$, which can be further divided into a linear part (i.e., $\frac{\sigma(x,t)}{E_S}$) and a nonlinear part (i.e., $\lambda_S \tanh\left(\frac{\sigma(x,t)}{\sigma_S}\right)$ when $\frac{\sigma(x,t)}{\sigma_S} \geqslant 0$, or $\frac{\lambda_S}{2}\tanh\left(\frac{2\sigma(x,t)}{\sigma_S}\right)$ when $\frac{\sigma(x,t)}{\sigma_S} < 0$), and describes the elastic property when $T(x, t) = T_r$ and $M(x, t) = 0$. The second consists of the terms dependent only the temperature $T(x, t)$ (i.e., $\alpha[T(x, t) - T_r]$), which describes the thermal expansion property when $\sigma(x, t) = 0$ and $M(x, t) = 0$. The third consists of the terms dependent on both the temperature $T(x, t)$ and the magnetization $M(x, t)$ (i.e., $-\frac{\tilde{B}}{M_S^2}[T(x,t) - T_r]M(x,t)^2$), which describes the nonlinear magnetic-thermal coupling property when $\sigma(x, t) = 0$. The fourth consists of the terms dependent on both the stress $\sigma(x, t)$ and the magnetization $M(x, t)$ (i.e., $\frac{\left[1-\tanh\left(\frac{\sigma(x,t)}{\sigma_S}\right)\right]\lambda_S}{M_S^2}M(x,t)^2$ when $\frac{\sigma(x,t)}{\sigma_S} \geqslant 0$, or $\frac{\left[2-\tanh\left(\frac{2\sigma(x,t)}{\sigma_S}\right)\right]\lambda_S}{2M_S^2}M(x,t)^2$ when $\frac{\sigma(x,t)}{\sigma_S} < 0$), which describes the nonlinear magnetic-elastic coupling property when $T(x, t) = T_r$. Thus, the effects of the magnetization $M(x, t)$ and temperature $T(x, t)$ on the strain $\varepsilon(x, t)$ are also incorporated in the nonlinear transient constitutive model. Here, the magnetostrictive strain $\lambda(x, t)$ in the conventional sense is induced by the applied magnetic field $H(t)$, which is dependent on the magnetization $M(x, t)$ in Eq. (3) and can be expressed as follows:

$$\lambda(x,t) = -\frac{\tilde{B}}{M_S^2}[T(x,t)-T_r]M(x,t)^2 + \begin{cases} \frac{\left[1-\tanh\left(\frac{\sigma(x,t)}{\sigma_S}\right)\right]\lambda_S}{M_S^2}M(x,t)^2 & \left(\frac{\sigma(x,t)}{\sigma_S} \geqslant 0\right) \\ \frac{\left[2-\tanh\left(\frac{2\sigma(x,t)}{\sigma_S}\right)\right]\lambda_S}{2M_S^2}M(x,t)^2 & \left(\frac{\sigma(x,t)}{\sigma_S} < 0\right) \end{cases} \tag{8}$$

For the convenience of the nonlinear transient constitutive model application in the derivation process of the dynamic model, Eq. (3) can be rewritten in a compact form

$$\varepsilon(x,t) = \frac{\sigma(x,t)}{E_S} + \vartheta(x,t) \tag{9}$$

where

$$\vartheta(x,t) = \alpha[T(x,t)-T_r] - \frac{\tilde{B}}{M_S^2}[T(x,t)-T_r]M(x,t)^2 + \begin{cases} \lambda_S\tanh\left(\frac{\sigma(x,t)}{\sigma_S}\right) + \frac{\left[1-\tanh\left(\frac{\sigma(x,t)}{\sigma_S}\right)\right]\lambda_S}{M_S^2}M(x,t)^2 & \left(\frac{\sigma(x,t)}{\sigma_S} \geqslant 0\right) \\ \frac{\lambda_S}{2}\tanh\left(\frac{2\sigma(x,t)}{\sigma_S}\right) + \frac{\left[2-\tanh\left(\frac{2\sigma(x,t)}{\sigma_S}\right)\right]\lambda_S}{2M_S^2}M(x,t)^2 & \left(\frac{\sigma(x,t)}{\sigma_S} < 0\right) \end{cases} \tag{10}$$

The direct use of the constitutive Eq. (2) or Eq. (9) yields an undamped dynamic model for the Terfenol-D rod. In such a case, a revised dynamic model can be obtained for the Terfenol-D rod by incorporating Kelvin–Voigt damping in Eq. (9), i.e.

$$\sigma(x,t) = E_S\varepsilon(x,t) + c_{k-v}\frac{\partial\varepsilon(x,t)}{\partial t} - E_S\vartheta(x,t) \tag{11}$$

for $0 < x < l$, in which c_{k-v} denotes Kelvin–Voigt damping coefficient. When integrated across the rod, the inplane resultant force $F(x, t)$ can be obtained

$$F(x,t) = S_0\sigma(x,t) \tag{12}$$

Direct substitution of geometrical Eq. (1) into Eq. (11) yields

$$\sigma(t,x) = E_S\frac{\partial u(x,t)}{\partial x} + c_{k-v}\frac{\partial^2 u(x,t)}{\partial x\partial t} - E_S\vartheta(x,t) \tag{13}$$

Substituting Eq. (13) into Eq. (12), then gives

$$F(x,t) = E_S S_0\frac{\partial u(x,t)}{\partial x} + c_{k-v}S_0\frac{\partial^2 u(x,t)}{\partial x\partial t} - E_S S_0\vartheta(x,t) \tag{14}$$

Based on the theorem of momentum, the model of the internal rod dynamics (i.e., wave equation) can be obtained, i.e.

$$\rho S_0\frac{\partial^2 u(x,t)}{\partial t^2} = \frac{\partial F(x,t)}{\partial x} \tag{15}$$

in which ρ denotes the density of the Terfenol-D rod.

At the fixed end of the Terfenol-D rod (i.e., $x = 0$), the boundary condition can be easily obtained, i.e.

$$u(0,t) = 0 \tag{16}$$

However, at the top-end of the Terfenol-D rod (i.e., $x = l$), the boundary condition is a general elastic boundary condition unlike the fixed end. The top-end, as depicted in Fig. 2, is constrained by the prestress spring washer which is modeled by a linear translational spring having stiffness K_l and damping coefficient C_l, and has an attached point mass M_l to model general loads encountered in applications. It is noted that due to the prestress bolt and spring washer, the Terfenol-D rod is subjected to a prestress σ_0 as shown in Fig. 2. After the prestress σ_0 is applied, the magnetically unloaded Terfenol-D rod will attain a new equilibrium sate, in which the elastic strain relative to unstressed state can be obtained according to Eq. (2), i.e.

$$\varepsilon_0 = \frac{\sigma_0}{E_S} + \begin{cases} \lambda_S\tanh\left(\frac{\sigma_0}{\sigma_S}\right) & \left(\frac{\sigma_0}{\sigma_S} \geqslant 0\right) \\ \frac{\lambda_S}{2}\tanh\left(\frac{2\sigma_0}{\sigma_S}\right) & \left(\frac{\sigma_0}{\sigma_S} < 0\right) \end{cases} \tag{17}$$

From Eq. (17), it can be found that, for the Terfenol-D rod, the elastic strain ε_0 induced only by the prestress σ_0 also includes a linear part (i.e., $\frac{\sigma_0}{E_S}$) and a nonlinear part (i.e., $\lambda_S\tanh\left(\frac{\sigma_0}{\sigma_S}\right)$ when

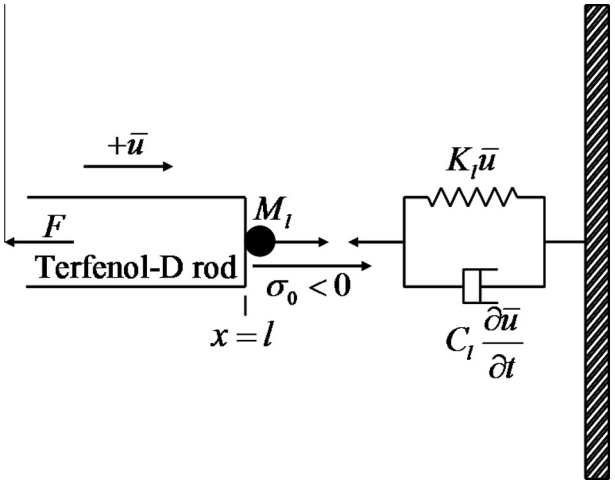

Fig. 2. Spring, damped oscillator, and point mass used to model loads in applications.

$\frac{\sigma_0}{\sigma_S} \geqslant 0$, or $\frac{\lambda_S}{2}\tanh\left(\frac{2\sigma_0}{\sigma_S}\right)$ when $\frac{\sigma_0}{\sigma_S} < 0$) unlike ordinary elastic materials, which can be used to describe the "overturn phenomenon" and ΔE effect of Terfenol-D observed in the experiments. The detailed discussion about these can be found in the reference (Zheng and Liu, 2005).

Under the assumption of homogeneous material properties and a uniform cross-section area, the displacement of the magnetically unloaded Terfenol-D rod relative to the unstressed state under the prestress equilibrium state can be obtained based on the geometrical Eq. (1), i.e.

$$u_0(x) = \varepsilon_0 x \tag{18}$$

for $0 \leqslant x \leqslant l$. In such a case, the time-dependent displacement relative to the prestress equilibrium state, denoted by $\bar{u}(x,t)$, can be given by the equation

$$\bar{u}(x,t) = u(x,t) - u_0(x) \tag{19}$$

Differentiating Eq. (19) with respect to the longitudinal coordinate x, and then substituting Eqs. (1) and (18) into the resulting one yields

$$\bar{\varepsilon}(x,t) = \varepsilon(x,t) - \varepsilon_0 \tag{20}$$

in which $\bar{\varepsilon}(x,t) = \frac{\partial \bar{u}(x,t)}{\partial x}$ denotes the total strain relative to the prestress equilibrium state. Here, it is noted that for a compressive prestress σ_0, ε_0 and subsequent $u_0(x)$ will be negative.

In order to obtain appropriate boundary conditions at the end $x = l$, we consider an infinitesimal section having the orientation shown in Fig. 2. The theorem of momentum over the infinitesimal section then yields the elastic boundary condition

$$F(l,t) = -K_l[u(l,t) - u_0(l)] - C_l\frac{\partial[u(l,t) - u_0(l)]}{\partial t} - M_l\frac{\partial^2[u(l,t) - u_0(l)]}{\partial t^2} + \sigma_0 S_0 \tag{21}$$

Substituting $u_0(l) = \varepsilon_0 l$ into Eq. (21) yields

$$F(l,t) = -K_l[u(l,t) - \varepsilon_0 l] - C_l\frac{\partial u(l,t)}{\partial t} - M_l\frac{\partial^2 u(l,t)}{\partial t^2} + \sigma_0 S_0 \tag{22}$$

The initial conditions for the giant magnetostrictive actuator system can be given as follows:

$$u(x,0) = \varepsilon_0 x \tag{23}$$

$$\frac{\partial u(x,0)}{\partial t} = 0 \tag{24}$$

in which the equilibrium displacement (i.e., $u_0(x)$) induced only by the prestress σ_0 is incorporated.

The nonlinear transient constitutive model expressed by Eqs. (2) and (3), the wave equation expressed by Eq. (15), the boundary conditions expressed by Eqs. (16) and (22), and the initial conditions expressed by Eqs. (23) and (24) can be combined to constitute a nonlinear dynamic model for the giant magnetostrictive actuator system, in which both the material coupling and the structural coupling are incorporated. Therefore, the nonlinear dynamic model established in this section can be used to describe the complex hysteresis behavior of the giant magnetostrictive actuator system under quasi-static operating conditions and under dynamic operating conditions. However, the analytic solution of the nonlinear dynamic model is not able to be obtained due to its strongly nonlinear multi-fields coupling characteristic. In such a case, an appropriate numerical arithmetic for approximating the solution of the nonlinear dynamic model is given in the next section.

3. Numerical arithmetic

In order to approximate the solution of the nonlinear dynamic model established in Section 2, we consider a uniform partition of the interval $[0,l]$ with nodes $x_i = ih$, $i = 0,1,2,\ldots,n$ and spatial step size $h = \frac{l}{n}$, where n denotes the number of subintervals (Shang et al., 2008). After that, a piecewise linear interpolation function $u_h(x,t)$ can be used to approximate the solution $u(x,t)$ of the nonlinear dynamic model for the giant magnetostrictive actuator system, which can be expressed as follows (Prenter, 1975):

$$u_h(x,t) = \sum_{i=1}^{n} N_i(x)u_i(t) \tag{25}$$

in which $u_i(t)$ denotes the node displacements, and $N_i(x)$ denotes the basis functions of the piecewise linear interpolation (Prenter, 1975), i.e.

$$N_i(x) = \frac{1}{h}\begin{cases}(x - x_{i-1}), & x_{i-1} < x \leqslant x_i \\ (x_{i+1} - x), & x_i < x \leqslant x_{i+1} \\ 0, & x \in [0,l], x \notin [x_{i-1}, x_{i+1}]\end{cases} \quad (i = 1,2,\ldots,n-1) \tag{26}$$

$$N_n(x) = \frac{1}{h}\begin{cases}(x - x_{n-1}) & x_{n-1} < x \leqslant x_n \\ 0, & x \in [0,l], x \notin [x_{n-1}, x_n]\end{cases} \tag{27}$$

From the expressions of the basis functions $N_i(x)$, one can find that the piecewise linear interpolation function $u_h(x,t)$ satisfies the boundary condition $u_h(0,t) = 0$ at $x = 0$ and allows arbitrary displacements at $x = l$.

Multiplying both sides of Eq. (15) by the basis functions $N_j(x)$, and then integrating the resulting equation along the x direction gives

$$\int_0^l \rho S_0 \frac{\partial^2 u(x,t)}{\partial t^2} N_j(x)dx = \int_0^l \frac{\partial F(x,t)}{\partial x} N_j(x)dx \quad (j = 1,2,\ldots,n) \tag{28}$$

With the aid of integration by parts, Eq. (28) can be written as follows:

$$\int_0^l \rho S_0 \frac{\partial^2 u(x,t)}{\partial t^2} N_j(x)dx = F(l,t)N_j(l) - F(0,t)N_j(0) - \int_0^l F(x,t)\frac{dN_j(x)}{dx}dx \quad (j = 1,2,\ldots,n) \tag{29}$$

Substituting Eqs. (14) and (22) as well as $N_j(0) = 0$ into Eq. (28) yields

$$\begin{aligned}&\int_0^l \rho S_0 \frac{\partial^2 u(x,t)}{\partial t^2} N_j(x)dx \\ &= \left\{-K_l[u(l,t) - \varepsilon_0 l] - C_l\frac{\partial u(l,t)}{\partial t} - M_l\frac{\partial^2 u(l,t)}{\partial t^2} + \sigma_0 S_0\right\} \times N_j(l) \\ &\quad - \int_0^l \left[E_S S_0 \frac{\partial u(x,t)}{\partial x} + c_{k-v} S_0 \frac{\partial^2 u(x,t)}{\partial x \partial t} - E_S S_0 \vartheta(x,t)\right]\frac{dN_j(x)}{dx}dx \\ &\quad \times (j = 1,2,\ldots,n)\end{aligned} \tag{30}$$

Replacing $u(x,t)$ by $u_h(x,t)$, substituting Eq. (25) into Eq. (30), and after some mathematical manipulations yield a set of the second-order time-dependent differential equations

$$\begin{aligned}&\sum_{i=1}^{n}\left[\int_0^l \rho S_0 N_i(x)N_j(x)dx + M_l N_i(l)N_j(l)\right]\ddot{u}_i(t) \\ &\quad + \sum_{i=1}^{n}\left[\int_0^l c_{k-v} S_0 \frac{dN_i(x)}{dx}\frac{dN_j(x)}{dx}dx + C_l N_i(l)N_j(l)\right]\dot{u}_i(t) \\ &\quad + \sum_{i=1}^{n}\left[\int_0^l E_S S_0 \frac{dN_i(x)}{dx}\frac{dN_j(x)}{dx}dx + K_l N_i(l)N_j(l)\right]u_i(t) \\ &= \int_0^l E_S S_0 \vartheta(x,t)\frac{dN_j(x)}{dx}dx + [K_l\varepsilon_0 l + \sigma_0 S_0]N_j(l) \quad (j = 1,2,\ldots,n)\end{aligned} \tag{31}$$

here, $\cdot$ denotes a temporal derivative, and Eq. (31) can be rewritten in the matrix form

$$[\boldsymbol{M}]\{\ddot{\boldsymbol{u}}(t)\}+[\boldsymbol{C}]\{\dot{\boldsymbol{u}}(t)\}+[\boldsymbol{K}]\{\boldsymbol{u}(t)\}=\{\boldsymbol{Q}(x,t)\} \tag{32}$$

in which $\{\boldsymbol{u}(t)\}$, $\{\dot{\boldsymbol{u}}(t)\}$ and $\{\ddot{\boldsymbol{u}}(t)\}$ are respectively the displacement vector, velocity vector and acceleration vector of node, and $[\boldsymbol{M}]$, $[\boldsymbol{C}]$ and $[\boldsymbol{K}]$ respectively denote the mass matrix, damping matrix and stiffness matrix. According to Eq. (31), one can find that these matrices have the components

$$M_{ij}=\int_0^l \rho S_0 N_i(x)N_j(x)dx+M_l N_i(l)N_j(l) \tag{33}$$

$$C_{ij}=\int_0^l c_{k-v}S_0\frac{dN_i(x)}{dx}\frac{dN_j(x)}{dx}dx+C_l N_i(l)N_j(l) \tag{34}$$

$$K_{ij}=\int_0^l E_S S_0\frac{dN_i(x)}{dx}\frac{dN_j(x)}{dx}dx+K_l N_i(l)N_j(l) \tag{35}$$

while the load vector $\{\boldsymbol{Q}(x,t)\}$ is integrated by

$$Q_j(x,t)=\int_0^l E_S S_0\vartheta(x,t)\frac{dN_j(x)}{dx}dx+[K_l\varepsilon_0 l+\sigma_0 S_0]N_j(l) \tag{36}$$

Here, based on Eq. (32), the acceleration vector $\{\ddot{\boldsymbol{u}}(0)\}$ at the initial moment $t=0$ is particularly expressed as follows:

$$\{\ddot{\boldsymbol{u}}(0)\}=[\boldsymbol{M}]^{-1}(\{\boldsymbol{Q}(x,0)\}-[\boldsymbol{C}]\{\dot{\boldsymbol{u}}(0)\}-[\boldsymbol{K}]\{\boldsymbol{u}(0)\}) \tag{37}$$

In order to solve the nonlinear dynamic differential Eq. (32) for the giant magnetostrictive actuator system, the Newmark method (Zhou et al., 2006) is here employed. After that, Eq. (32) is converted into the following difference equation:

$$[\boldsymbol{M}]\{\ddot{\boldsymbol{u}}(t+\Delta t)\}+[\boldsymbol{C}]\{\dot{\boldsymbol{u}}(t+\Delta t)\}+[\boldsymbol{K}]\{\boldsymbol{u}(t+\Delta t)\}=\{\boldsymbol{Q}(x,t+\Delta t)\} \tag{38}$$

where

$$\{\dot{\boldsymbol{u}}(t+\Delta t)\}=\{\dot{\boldsymbol{u}}(t)\}+[(1-\delta)\{\ddot{\boldsymbol{u}}(t)\}+\delta\{\ddot{\boldsymbol{u}}(t+\Delta t)\}]\Delta t \tag{39}$$

$$\{\boldsymbol{u}(t+\Delta t)\}=\{\boldsymbol{u}(t)\}+\{\dot{\boldsymbol{u}}(t)\}\Delta t+\left[\left(\frac{1}{2}-\xi\right)\{\ddot{\boldsymbol{u}}(t)\}+\xi\{\ddot{\boldsymbol{u}}(t+\Delta t)\}\right]\Delta t^2 \tag{40}$$

(see (Zhou et al., 2006)), here, Δt is the temporal step size, and δ and ξ are the parameters of the Newmark method.

Substituting Eqs. (39) and (40) into Eq. (38), and after some simple mathematical manipulations, we get the algebraic iterative equation at the moment $t+\Delta t$, i.e.

$$\begin{aligned}&([\boldsymbol{M}]+\delta\Delta t[\boldsymbol{C}]+\xi\Delta t^2[\boldsymbol{K}])\{\ddot{\boldsymbol{u}}(t+\Delta t)\}\\&=\{\boldsymbol{Q}(x,t+\Delta t)\}-[\boldsymbol{C}][\{\dot{\boldsymbol{u}}(t)\}+(1-\delta)\Delta t\{\ddot{\boldsymbol{u}}(t)\}]\\&\quad-[\boldsymbol{K}]\left[\{\boldsymbol{u}(t)\}+\Delta t\{\dot{\boldsymbol{u}}(t)\}+\left(\frac{1}{2}-\xi\right)\Delta t^2\{\ddot{\boldsymbol{u}}(t)\}\right]\end{aligned} \tag{41}$$

Eq. (41) can be written in a compact form

$$[\hat{\boldsymbol{M}}]\{\ddot{\boldsymbol{u}}(t+\Delta t)\}=\{\hat{\boldsymbol{Q}}(x,t+\Delta t)\} \tag{42}$$

in which the equivalent mass matrix $[\hat{\boldsymbol{M}}]$ and the equivalent load vector $\{\hat{\boldsymbol{Q}}(x,t+\Delta t)\}$ can be respectively expressed as follows:

$$[\hat{\boldsymbol{M}}]=[\boldsymbol{M}]+c_0[\boldsymbol{C}]+c_1[\boldsymbol{K}] \tag{43}$$

$$\begin{aligned}\{\hat{\boldsymbol{Q}}(x,t+\Delta t)\}&=\{\boldsymbol{Q}(x,t+\Delta t)\}-[\boldsymbol{C}][\{\ddot{\boldsymbol{u}}(t)\}+c_2\{\ddot{\boldsymbol{u}}(t)\}]-[\boldsymbol{K}]\\&\quad\times[\{\boldsymbol{u}(t)\}+\Delta t\{\dot{\boldsymbol{u}}(t)\}+c_3\{\ddot{\boldsymbol{u}}(t)\}]\end{aligned} \tag{44}$$

here, $c_0=\delta\Delta t$, $c_1=\xi\Delta t^2$, $c_2=(1-\delta)\Delta t$ and $c_3=(\frac{1}{2}-\xi)\Delta t^2$.

From Eqs. (33)–(35) as well as Eq. (43), one can find that the equivalent mass matrix $[\hat{\boldsymbol{M}}]$ and its inverse matrix $[\hat{\boldsymbol{M}}]^{-1}$ need only be created once in the following numerically calculation. It significantly enhances the computational efficiency of the model compared with the references Sun and Zheng (2006) and Zhou et al. (2006). In these references Sun and Zheng (2006) and Zhou et al. (2006), the corresponding equivalent matrices and their inverse matrices must be recreated within every iteration step due to ΔE effect, which increases implementation time of the model and will limit flexibility if employed in a control law. Meanwhile, based on Eq. (41), (42), we know that $\{\ddot{\boldsymbol{u}}(t+\Delta t)\}$ at the moment $t+\Delta t$ can be obtained easily once the quantities $\{\boldsymbol{u}(t)\}$, $\{\dot{\boldsymbol{u}}(t)\}$ and $\{\ddot{\boldsymbol{u}}(t)\}$ at the moment t as well as the load vector $\{\boldsymbol{Q}(x,t+\Delta t)\}$ at the moment $t+\Delta t$ are known. Then $\{\dot{\boldsymbol{u}}(t+\Delta t)\}$ and $\{\boldsymbol{u}(t+\Delta t)\}$ at the moment $t+\Delta t$ can be calculated by Eqs. (39) and (40), respectively. However, from Eq. (36), it can be found that the load vector $\{\boldsymbol{Q}(x,t+\Delta t)\}$ is relative to $\vartheta(x,t+\Delta t)$, which is nonlinearly dependent on the unknowns $\sigma(x,t+\Delta t)$ at the moment $t+\Delta t$ as shown in Eq. (10). And $\sigma(x,t+\Delta t)$ is determined by $\vartheta(x,t+\Delta t)$ and $\{\boldsymbol{u}(t+\Delta t)\}$ at the moment $t+\Delta t$ according to Eq. (13). Therefore, it is a strongly nonlinear coupling problem just as shown in the previous sections. In order to solve this nonlinear coupling problem, here, an iteration process is employed. The main steps of the program are briefly introduced as follows:

Step 1. Specify the number n of subintervals, and then form the mass matrix $[\boldsymbol{M}]$, damping matrix $[\boldsymbol{C}]$, and stiffness matrix $[\boldsymbol{K}]$. The mass, damping and stiffness matrices are integrated based on Eqs. (33)–(35), respectively.

Step 2. Input the prestress σ_0 and temperature $T(x,t)$, which is fixed in the following numerically calculation, as well as initial values of $\{\boldsymbol{u}(0)\}$ and $\{\dot{\boldsymbol{u}}(0)\}$ according to the initial conditions of the Terfenol-D rod at the moment $t=0$. After that, the acceleration vector $\{\ddot{\boldsymbol{u}}(0)\}$ at the moment $t=0$ is calculated by Eq. (37).

Step 3. Choose the temporal step size Δt and the parameters (i.e., δ and ξ) of the Newmark method, which are taken as $\delta=0.5$ and $\xi=0.25(0.5+\delta)$ in the following numerically calculation to satisfy stability requirements. Then, the constants $c_0=\delta\Delta t$, $c_1=\xi\Delta t^2$, $c_2=(1-\delta)\Delta t$ and $c_3=(\frac{1}{2}-\xi)\Delta t^2$ are calculated.

Step 4. Form the equivalent mass matrix $[\hat{\boldsymbol{M}}]$ based on Eq. (43).

Step 5. Assume an initial iteration value of $\sigma^{(r)}(x,t+\Delta t)$. Here, the increment method is used to select the initial iteration value, i.e., $\sigma^{(r)}(x,t+\Delta t)=\sigma(x,t)$, and the superscript r means the step of iteration.

Step 6. Calculate the magnetization $M(x,t+\Delta t)$ at the moment $t+\Delta t$. The influence of the stress $\sigma(x,t)$ on the magnetization $M(x,t)$ is accomplished by the rate of change in the magnetization with time $\frac{\partial M(x,t)}{\partial t}$ in Eq. (3). Eq. (3) is a nonlinear equation, and the Newton–Raphson method is adopted to solve Eq. (3) for $\frac{\partial M(x,t)}{\partial t}$. After $\frac{\partial M(x,t)}{\partial t}$ is obtained, the Adams-type predictor-corrector method is employed to calculate the magnetization $M(x,t+\Delta t)$ at the moment $t+\Delta t$.

Step 7. Calculate the load vector $\{\boldsymbol{Q}(x,t+\Delta t)\}$ at the moment $t+\Delta t$. The load vector $\{\boldsymbol{Q}(x,t+\Delta t)\}$ is integrated based on Eq. (36). The variable $\vartheta(x,t+\Delta t)$ in Eq. (36) is calculated by Eq. (10). As shown in Eq. (10), it is obvious that $\vartheta(x,t+\Delta t)$ is nonlinearly dependent on both the stress $\sigma(x,t+\Delta t)$ and magnetization $M(x,t+\Delta t)$ at the moment $t+\Delta t$ when the temperature $T(x,t+\Delta t)$ is fixed. And it is directly calculated after $\sigma(x,t+\Delta t)=\sigma^{(r)}(x,t+\Delta t)$ is assumed and $M(x,t+\Delta t)$ is obtained at step 6.

Step 8. Form the equivalent load vector $\{\hat{\boldsymbol{Q}}(x,t+\Delta t)\}$ based on Eq. (44).

Step 9. Calculate the acceleration vector $\{\ddot{\boldsymbol{u}}(t+\Delta t)\}$, velocity vector $\{\dot{\boldsymbol{u}}(t+\Delta t)\}$ and displacement vector $\{\boldsymbol{u}(t+\Delta t)\}$at the moment $t+\Delta t$. The acceleration vector $\{\ddot{\boldsymbol{u}}(t+\Delta t)\}$ is calculated based on Eq. (42). After that, the velocity vector $\{\dot{\boldsymbol{u}}(t+\Delta t)\}$ and displacement vector $\{\boldsymbol{u}(t+\Delta t)\}$ is calculated by Eqs. (39) and (40), respectively.

Step 10. Calculate the stress $\sigma(x,t+\Delta t)$ at the moment $t+\Delta t$. A modified stress $\sigma^{(r+1)}(x,t+\Delta t)$ at the moment $t+\Delta t$ is calculated by Eq. (13) when $u(x,t+\Delta t)$ is replaced by $u_h(x,t+\Delta t)$. After that the absolute error $\|\sigma^{(r+1)}(x,t+\Delta t)-\sigma^{(r)}(x,t+\Delta t)\|$ is calculated. If the precision condition $\|\sigma^{(r+1)}(x,t+\Delta t)-\sigma^{(r)}(x,t+\Delta t)\|<\delta_1$ is not satisfied, $\sigma^{(r)}(x,t+\Delta t)$ is replaced by $\sigma^{(r+1)}(x,t+\Delta t)$ and the program goes to step 7 until the precision condition is satisfied; otherwise, $\sigma^{(r+1)}(x,t+\Delta t)$ is the true stress of the Terfenol-D rod at the moment $t+\Delta t$, i.e., $\sigma(x,t+\Delta t)=\sigma^{(r+1)}(x,t+\Delta t)$. Here, δ_1 is a small positive number of specific accuracy.

Step 11. Calculate the total strain $\varepsilon(x,t+\Delta t)$ relative to the unstressed state and magnetostrictive strain $\lambda(x,t+\Delta t)$ at the moment $t+\Delta t$. The total strain $\varepsilon(x,t+\Delta t)$ and magnetostrictive strain $\lambda(x,t+\Delta t)$ are calculated by Eqs. (1) and (8), respectively.

Step 12. Replace t by $t+\Delta t$, and repeat the above steps 5–11, the correlative physical quantities such as the displacement, velocity, acceleration, stress, strain, magnetization and magnetostrictive strain at any moment can be calculated.

We conclude this section by noting that two kinds of strain are calculated in the above numerical arithmetic. They are the magnetostrictive strain $\lambda(x,t)$ and total strain $\varepsilon(x,t)$ relative to the unstressed state, respectively. However, the total strain $\bar{\varepsilon}(x,t)$ relative to the prestress equilibrium state is usually measured in the experiments (Liang and Zheng, 2007; Slaughter et al., 2000; Faidley et al., 1998), which is easily calculated by Eq. (20). In such a case, unless otherwise noted, when the total strain is mentioned in the following sections it will refer to the total strain $\bar{\varepsilon}(x,t)$ relative to the prestress equilibrium state.

4. Experimental verification and discussion

In order to verify the validity and reliability of the nonlinear dynamic model and corresponding numerical approximation method proposed in Section 2 and Section 3, in this section, quantitative comparisons between its predictions and Slaughter et al. (2000) experimental data are firstly given. After that, the differences between the magnetostrictive strain and total strain, and the influences of the eddy current effects and structural dynamic behavior on the hysteresis behavior of the giant magnetostrictive actuator system under magnetically unbiased conditions are discussed in detail by using this nonlinear dynamic model.

To comply with the experimental conditions (Slaughter et al., 2000), the prestress and temperature are respectively taken as $\sigma_0=-1500$psi and $T(x,t)=18\ ^\circ$C, the applied magnetic field H is a fixed-frequency sinusoidal driving magnetic field (i.e., $H(t)=H_{amp}\sin(2\pi ft)$), and the amplitudes of applied magnetic field are respectively taken as $H_{amp}=110$ kA/m when the exciting frequency $f=1$ Hz and $H_{amp}=20$ kA/m when $f=1000$ Hz. The material parameters appeared in the nonlinear transient constitutive model are given as $M_S=7.65\times10^5$ A/m, $\tilde{B}=2.5\times10^{-6}\ ^\circ\mathrm{C}^{-1}$, $\lambda_S=1950\times10^{-6}$, $\alpha=1.2\times10^{-5}\ ^\circ\mathrm{C}^{-1}$, $\sigma_S=200\times10^6$ Pa, $\eta=0.082$, $\theta=4.3\times10^{-6}\Omega$ m, $\chi_m=20.4$, $K=6000$ A/m, $H_0=0.03$ A/m, $c=0.1$ and $D=12.7\times10^{-3}$ m, which are used in succeeding numerical simulations and in accordance with the parameters given in the references Cao et al. (2006), Slaughter et al. (2000), Wang and Zhou (2011). The computational time taken by the nonlinear dynamic model to simulate the Slaughter et al. (2000) experimental data under different exciting frequencies is less then 0.5 s when it is implemented in MATLAB program. The comparisons between the numerical simulation results predicted by the nonlinear dynamic model and Slaughter et al. (2000) experimental data under quasi-static operating conditions are shown in Figs. 3 and 4. And the corresponding comparisons under dynamic operating conditions are shown in Figs. 5 and 6. As is evident in these four figures, the numerical simulation results are perfectly coincident with the experimental data not only for the relative magnetization hysteresis loops shown in Figs. 3 and 5 but also for the total strain hysteresis loops shown in Figs. 4 and 6. It confirms that the nonlinear dynamic model established in this paper can quantitatively describe the complex hysteresis behavior of the giant magnetostrictive actuator system under quasi-static operating conditions and under dynamic operating conditions, especially for the hysteresis behavior under high frequency dynamic operating conditions.

In practical application for the giant magnetostrictive actuators, ones mainly pay their attention to the strain hysteresis loop, which is also usually measured in the experiments. In this case, the differences between the magnetostrictive strain and total strain are firstly investigated by using the nonlinear dynamic model. Figs. 7 and 8 give out the comparisons between the magnetostrictive strain and total strain under quasi-static operating conditions and under dynamic operating conditions, respectively, in which the experimental data is also illustrated for reference. As shown in Fig. 7, the difference between the magnetostrictive strain and total strain under quasi-static operating conditions is small enough to be ignored. Both of them can quantitatively trace out the experimental hysteresis loop under quasi-static operating conditions. However, it is not the same under dynamic operating conditions. Because, under dynamic operating conditions, the experimental hysteresis loop can only be quantitatively fitted by the total strain hysteresis loop and the magnetostrictive strain hysteresis loop underestimates both the amplitude and energy losses of the strain hysteresis loop measured in the experiment as shown in Fig. 8. Therefore, the total strain hysteresis loops are mainly discussed in the following section.

In order to reflect the influences of the eddy current effects on the hysteresis behavior of the giant magnetostrictive actuator system under quasi-static operating conditions and under dynamic operating conditions, here, we ignore the eddy current effects and compare its predictions with Slaughter et al. experimental data in Figs. 9 and 10, in which the original predictions with the eddy current effects are also illustrated for reference. It is obvious in Fig. 9 that there is no influence of the eddy current effects on the total strain hysteresis loop under quasi-static operating conditions. However, the theoretical prediction without the eddy current effects markedly overestimates the amplitude of the total strain hysteresis loop under dynamic operating conditions, while the energy loss is underestimated, as shown in Fig. 10. Thus, in order to accurately capture hysteresis characteristic of the giant magnetostrictive actuator system in a broad range of the operating frequency, the eddy current effects including in the material coupling must

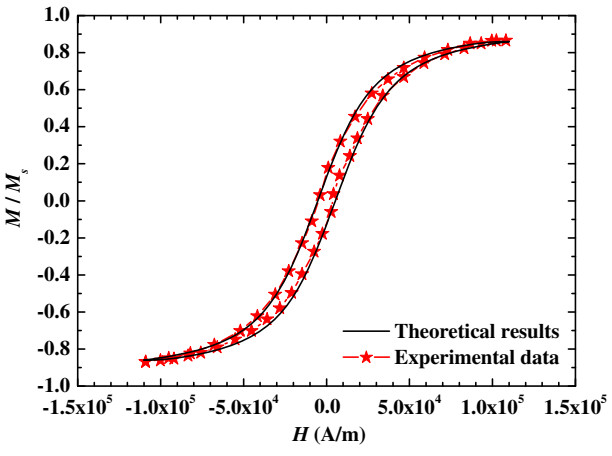

Fig. 3. Comparison of relative magnetization hysteresis loop between experimental measurements and theoretical predictions under quasi-static operating conditions.

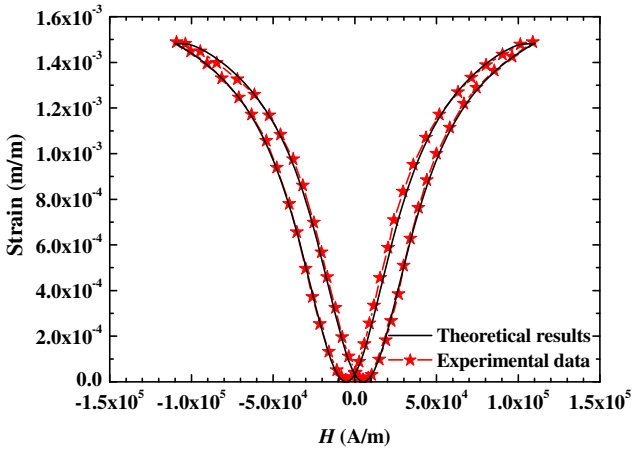

Fig. 4. Comparison of total strain hysteresis loop between experimental measurements and theoretical predictions under quasi-static operating conditions.

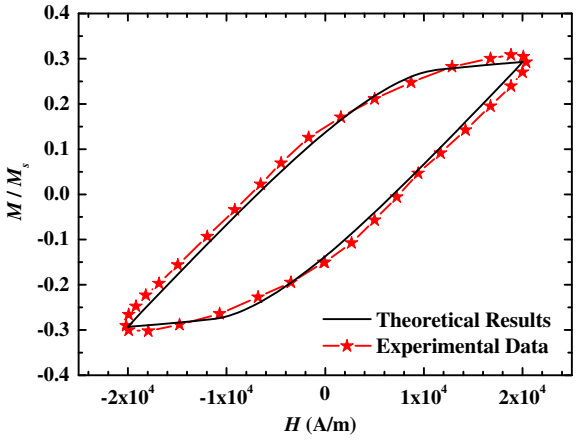

Fig. 5. Comparison of relative magnetization hysteresis loop between experimental measurements and theoretical predictions under dynamic operating conditions.

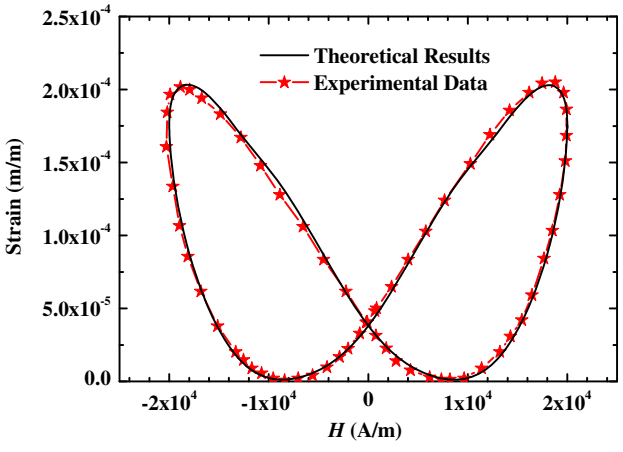

Fig. 6. Comparison of total strain hysteresis loop between experimental measurements and theoretical predictions under dynamic operating conditions.

be incorporated into the nonlinear dynamic model, which supports the conclusion of the references Wang and Zhou (2010), and Xu et al. (2013). The similar numerical analysis method is used to reflect the influences of the structural dynamic behavior on the hysteresis

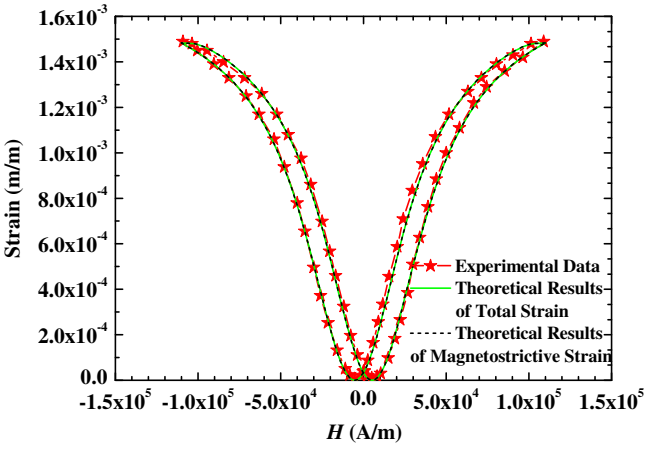

Fig. 7. Comparison between magnetostrictive strain hysteresis loop and total strain hysteresis loop under quasi-static operating conditions. The corresponding experimental data is illustrated for reference.

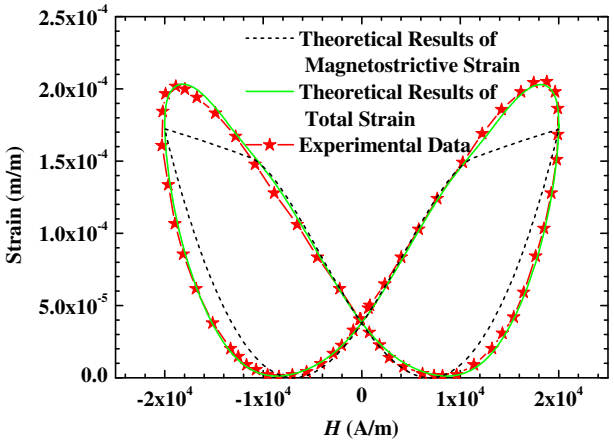

Fig. 8. Comparison between magnetostrictive strain hysteresis loop and total strain hysteresis loop under dynamic operating conditions. The corresponding experimental data is illustrated for reference.

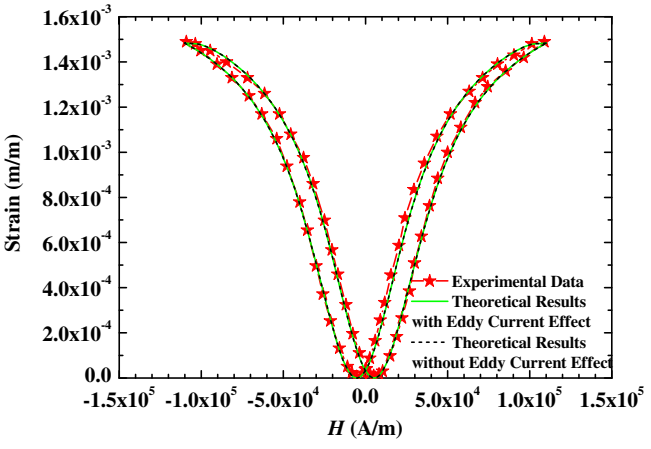

Fig. 9. Comparison of total strain hysteresis loop between experimental measurements and theoretical predictions without eddy current effects under quasi-static operating conditions. The corresponding theoretical predictions with eddy current effects are illustrated for reference.

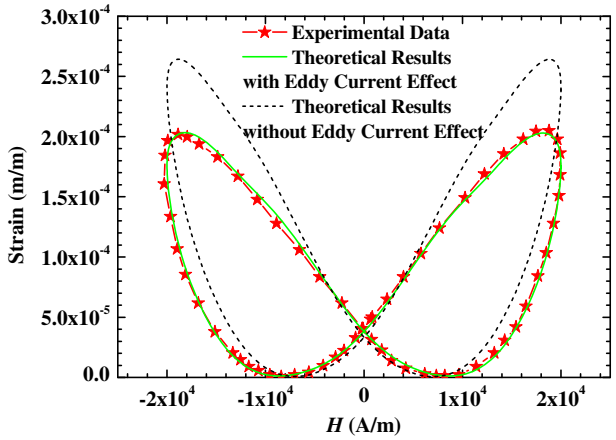

Fig. 10. Comparison of total strain hysteresis loop between experimental measurements and theoretical predictions without eddy current effects under dynamic operating conditions. The corresponding theoretical predictions with eddy current effects are illustrated for reference.

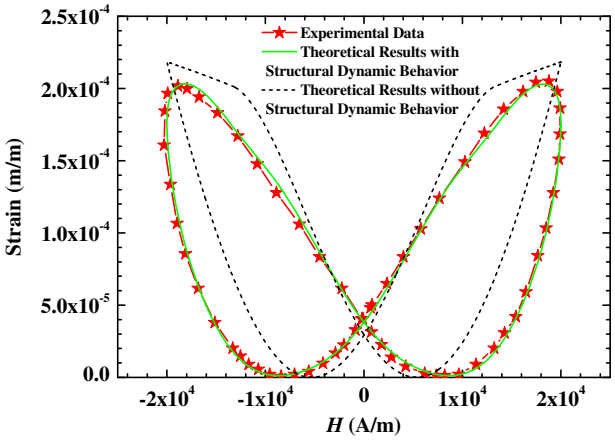

Fig. 12. Comparison of total strain hysteresis loop between experimental measurements and theoretical predictions without structural dynamic behavior under dynamic operating conditions. The corresponding theoretical predictions with structural dynamic behavior are illustrated for reference.

behavior of the giant magnetostrictive actuator system under quasi-static operating conditions and under dynamic operating conditions, as shown in Figs. 11 and 12. Just like the influence of the eddy current effects, the influence of the structural dynamic behavior on the hysteresis behavior is very tiny under quasi-static operating conditions, but the structural dynamic behavior reduces the amplitude and increases the energy loss of the total strain hysteresis loop under dynamic operating conditions as shown in Fig. 12. From the analysis of Figs. 10 and 12, one can find that both the eddy current effects and structural dynamic behavior are responsible for the frequency-dependent hysteresis behavior of the total strain observed in the experiment. Especially for the structural dynamic behavior, it causes the mechanical hysteresis loss of the giant magnetostrictive actuator system, which is detailedly reflected in Fig. 13. Fig. 13 gives out the predicted curve of the total strain as a function of the magnetization under dynamic operating conditions. From Fig. 13, one can see that the relationship between the total strain and magnetization exhibits nonlinear hysteresis characteristic, which is coincident with the experimental phenomenon observed under quasi-static operating conditions in qualitatively (Dapino et al., 2000b; Valadkhan et al., 2010). Meanwhile, this kind of hysteresis behavior is totally caused by the structural dynamic behavior of the giant magnetostrictive

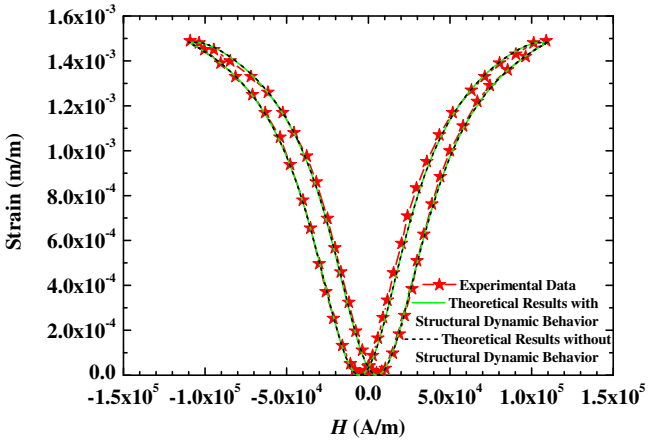

Fig. 11. Comparison of total strain hysteresis loop between experimental measurements and theoretical predictions without structural dynamic behavior under quasi-static operating conditions. The corresponding theoretical predictions with structural dynamic behavior are illustrated for reference.

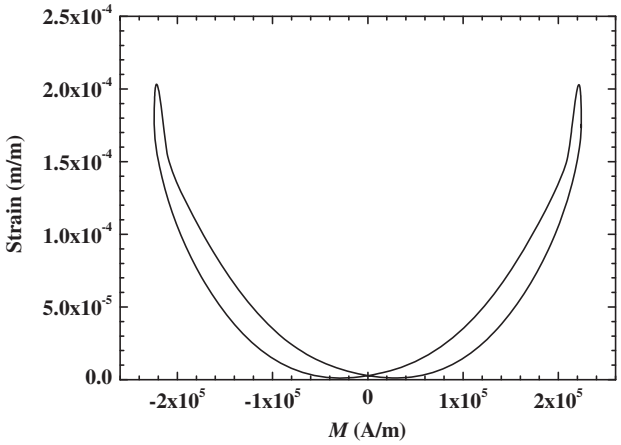

Fig. 13. Hysteresis loop of total strain versus magnetization under dynamic operating conditions.

actuator system, and leads to highly accurate model fit observed in Figs. 6 or 12. Therefore, the structural dynamic behavior reflecting the system-lever coupling plays an important role and can not be neglected under dynamic operating conditions. Based on the above analysis, we can conclude that the wide applicability and high precision of the nonlinear dynamic model mainly derive from simultaneously incorporating the material coupling and structural coupling when the model is established.

5. Conclusions

Based on the nonlinear transient constitutive model with eddy current effects of Terfenol-D, a novel general nonlinear dynamic model with multi-fields coupling effects is established in this paper for the giant magnetostrictive actuator system, in which strong coupling interaction between the nonlinear constitutive behavior of Terfenol-D and the structural dynamic behavior of actuator system itself is modeled through theorem of momentum. In this system-lever coupled theoretical model, the change of stress is characterized through the structural dynamic behavior of actuator system itself, and the eddy current effect is included in the nonlinear transient constitutive model, which can also reflect the effect of varied stress on the effective magnetic field and ensuing magnetization. The validity and reliability of the obtained nonlinear dy-

namic model are verified by quantitatively comparing its predicted results with existing experimental data. The excellent agreements between the predicted results and experimental data indicate that nonlinear dynamic model established in this paper can accurately describe the complex hysteresis behavior of the giant magnetostrictive actuator system not only under quasi-static operating conditions but also under dynamic operating conditions. On this basis, this paper calculates and analyzes the differences between the magnetostrictive strain and total strain, and the influences of the eddy current effects and structural dynamic behavior on the hysteresis behavior of the giant magnetostrictive actuator system under magnetically unbiased conditions. The numerical simulation results indicate the differences and influences mentioned above are tiny enough to be ignored under quasi-static operating conditions. However, under dynamic operating conditions, the difference between the magnetostrictive strain and total strain is very obvious, and both the eddy current effects and structural dynamic behavior are responsible for the frequency-dependent hysteresis behavior of the giant magnetostrictive actuator system, which lead to highly accurate model fit. All of these demonstrate the significance and necessity of simultaneously incorporating the material coupling and structural coupling in the nonlinear dynamic model. Therefore, the research of this paper provides a basic theoretical model for accurate characterization of the giant magnetostrictive actuators, which can be used in model-based active vibration control design.

Acknowledgements

This research was supported by a grant of the Key Fund of Natural Science Foundation of China (Grant No. 11032006), the Innovation Team Fund of Natural Science Foundation of China (Grant No. 11121202), the Fund of Natural Science Foundation of China (Grant No. 10972094), the Science Foundation of the Ministry of Education of China for the Ph.D. program, and the Scholarship Award for Excellent Doctoral Student granted by Ministry of Education. The authors gratefully acknowledge these supports. The authors also thank the reviews very much for their kind suggestions and useful comments.

References

Al-Jiboory, M., Lord, D.G., 1990. Study of the magnetostrictive distortion in single crystal Terfenol-D by X-ray diffraction. IEEE Trans. Magn. 26 (8), 2583–2585.

Armstrong, W.D., 1997. Magnetization and magnetostriction processes in $Tb_{(0.27-0.30)}Dy_{(0.73-0.70)}Fe_{(1.9-2.0)}$. J. Appl. Phys. 81, 2321–2326.

Bottauscio, O., Chiampi, M., Lovisolo, A., Roccato, P.E., Zucca, M., 2008. Dynamic modeling and experimental analysis of Terfenol-D rods for magnetostrictive actuators. J. Appl. Phys. 103, 07F121.

Calkins, F.T., Dapino, M.J., Flatau, A.B., 1997. Effect of prestress on the dynamic performance of a Terfenol-D transducer. Proc. SPIE 3041, 293–305.

Cao, S.Y., Wang, B.W., Zheng, J.J., Huang, W.M., Sun, Y., Yang, Q.X., 2006. Modeling dynamic hysteresis for giant magnetostrictive actuator using hybrid genetic algorithm. IEEE Trans. Magn. 42, 911–914.

Chakrabarti, S., Dapino, M.J., 2010. A dynamic model for a displacement amplified magnetostrictive driver for active mounts. Smart Mater. Struct. 19, 055009.

Chakrabarti, S., Dapino, M.J., 2012a. Fully coupled discrete energy-averaged model for Terfenol-D. J. Appl. Phys. 111, 054505.

Chakrabarti, S., Dapino, M.J., 2012b. Coupled axisymmetric finite element model of a hydraulically amplified magnetostrictive actuator for active powertrain mounts. Finite Elem. Anal. Des. 60, 25–34.

Clark, A.E., Crowder, D.N., 1985. High temperature magnetostriction of $TbFe_2$ and $Tb_{0.27}Dy_{0.73}Fe_2$. IEEE Trans. Magn. 21, 1945–1947.

Clark, A.E., Teter, J.P., McMasters, O.D., 1988. Magnetostriction "jumps" in twinned $Tb_{0.3}Dy_{0.7}Fe_{1.9}$. J. Appl. Phys. 63, 3910–3912.

Dapino, M.J., Smith, R.C., Faidley, L.E., Flatau, A.B., 2000a. A coupled structural-magnetic strain and stress model for magnetostrictive transducers. J. Intell. Mater. Syst. Struct. 11, 135–152.

Dapino, M.J., Smith, R.C., Flatau, A.B., 2000b. Structural magnetic strain model for magnetostrictive transducers. IEEE Trans. Magn. 36, 545–556.

Dapino, M.J., Smith, R.C., Calkins, F.T., Flatau, A.B., 2002. A coupled magnetomechanical model for magnetostrictive transducers and its application to Villari-effect sensors. J. Intell. Mater. Syst. Struct. 13, 737–747.

Dhilsha, K.R., Rama Rao, K.V.S., 1993. Investigation of magnetic magnetomechanical, and electrical properties of the $Tb_{0.27}Dy_{0.73}Fe_{2-x}Co_x$ system. J. Appl. Phys. 73, 1380–1385.

Evans, P.G., Dapino, M.J., 2011. Dynamic model for 3-D magnetostrictive transducers. IEEE Trans. Magn. 47, 221–230.

Faidley, L.E., Lund, B.J., Flatau, A.B., Calkins, F.T., 1998. Terfenol-D elasto-magnetic properties under varied operating conditions using hysteresis loop analysis. Proc. SPIE 3329, 856–865.

Gao, X., Pei, Y.M., Fang, D.N., 2008. Magnetomechanical behaviors of giant magnetostrictive materials. Acta Mech. Solida Sin. 21, 15–18.

Graham, F.C., Mudivarthi, C., Datta, S., Flatau, A.B., 2009. Modeling of a Galfenol transducer using the bidirectionally coupled magnetoelastic model. Smart Mater. Struct. 18, 104013.

Grunwald, A., Olabi, A.G., 2008. Design of a magnetostrictive (MS) actuator. Sens. Actuator A 144, 161–175.

Hirsinger, L., Billardon, R., 1995. Magneto-elastic finite element analysis including magnetic forces and magnetostriction effects. IEEE Trans. Magn. 31, 1877–1880.

Iyer, R.V., Krishnaprasad, P.S., 2005. On a low-dimensional model for ferromagnetism. Nonlinear Anal. 61, 1447–1482.

Jiles, D.C., 1994. Modeling the effects of eddy current losses on frequency dependent hysteresis in electrically conducting media. IEEE Trans. Magn. 30, 4326–4328.

Jiles, D.C., Atherton, D.L., 1986. Theory of ferromagnetic hysteresis. J. Magn. Magn. Mater. 61, 48–60.

Johnson, B.G., Avakian, K., Boudreau, D., Fenn, R.C., Gaffney, M.S., Gerver, M., Hawkey, T., 1992. Development of magnetostrictive active members for control of space structures. NASA, Report No. CR-190846.

Kannan, K.S., Dasgupta, A., 1997. A nonlinear Galerkin finite-element theory for modeling magnetostrictive smart structures. Smart Mater. Struct. 6, 341–350.

Liang, Y.R., Zheng, X.J., 2007. Experimental researches on magneto-thermo-mechanical characterization of Terfenol-D. Acta Mech. Solida Sin. 20, 283–288.

Lovisolo, A., Roccato, P.E., Zucca, M., 2008. Analysis of a magnetostrictive actuator equipped for the electromagnetic and mechanical dynamic characterization. J. Magn. Magn. Mater. 320, e915–e919.

Mahadevan, A., Evans, P.G., Dapino, M.J., 2010. Dependence of magnetic susceptibility on stress in textured polycrystalline $Fe_{81.6}Ga_{18.4}$ and $Fe_{79.1}Ga_{20.9}$ Galfenol alloys. Appl. Phys. Lett. 96, 012502.

Moffett, M.B., Clark, A.E., Wun-Fogle, M., Linberg, J., Teter, J.P., McLaughlin, E.A., 1991. Characterization of Terfenol-D for magnetostrictive transducers. J. Acoust. Soc. Am. 89, 1448–1455.

Nealis, J.M., Smith, R.C., 2007. Model-based robust control design for magnetostrictive transducers operating in hysteretic and nonlinear regimes. IEEE Trans. Control Syst. Techol. 15, 22–39.

Olabi, A.G., Grunwald, A., 2008. Design and application of magnetostrictive materials. Mater. Des. 29, 469–483.

Pérez-Aparicio, J.L., Sosa, H., 2004. A continuum three-dimensional, fully coupled, dynamic, non-linear finite element formulation for magnetostrictive materials. Smart Mater. Struct. 13, 493–502.

Pradhan, S.C., 2005. Vibration suppression of FGM shells using embedded magnetostrictive layers. Int. J. Solids Struct. 42, 2465–2488.

Prenter, P.M., 1975. Splines and Variational Methods. Wiley, New York.

Reimers, A., Torre, E.D., 1999. Fast preisach based magnetosriction model for highly magnetostrictive materials. IEEE Trans. Magn. 35, 1239–1242.

Sarawate, N.N., Dapino, M.J., 2008. A dynamic actuation model for magnetostrictive materials. Smart Mater. Struct. 17, 065013.

Shang, X.C., Pan, E., Qin, L.P., 2008. Mathematical modeling and numerical computation for the vibration of a magnetostrictive actuator. Smart Mater. Struct. 17, 045026.

Slaughter, J.C., 2009. Coupled structural and magnetic models: linear magnetostriction in comsol. In: Proceedings of COMSOL Conference Boston.

Slaughter, J.C., Dapino, M.J., Smith, R.C., Flatau, A.B., 2000. Modeling of a Terfenol-D ultrasonic transducer. Proc. SPIE 3985, 366–377.

Smith, R.C., Seelecke, S., Dapino, M., Ounaies, Z., 2006. A unified framework for modeling hysteresis in ferroic materials. J. Mech. Phys. Solids 54, 46–85.

Sun, L., Zheng, X.J., 2006. Numerical simulation on coupling behavior of Terfenol-D rods. Int. J. Solids Struct. 43, 1613–1623.

Tan, X.B., Baras, J.S., 2004. Modeling and control of hysteresis in magnetostrictive actuators. Automatica 40, 1469–1480.

Valadkhan, S., Morris, K., Shum, A., 2010. A new load-dependent hysteresis model for magnetostrictive materials. Smart Mater. Struct. 19, 125003.

Wang, T.Z., Zhou, Y.H., 2010. A nonlinear transient constitutive model with eddy current effects for giant magnetostrictive materials. J. Appl. Phys. 108, 123905.

Wang, T.Z., Zhou, Y.H., 2011. A coupled magnetic-elastic-thermal free-energy model with hysteresis nonlinearity for Terfenol-D rods. CMC-Comput. Mater. Con. 21, 41–64.

Xu, H., Pei, Y.M., Fang, D.N., Ai, S.G., 2013. An energy-based dynamic loss hysteresis model for giant magnetostrictive materials. Int. J. Solids Struct. 50, 672–679.

Zheng, X.J., Liu, X.E., 2005. A nonlinear constitutive model for Terfenol-D rods. J. Appl. Phys. 97, 053901.

Zheng, J.J., Cao, S.Y., Wang, H.L., Huang, W.W., 2007. Hybrid genetic algorithms for parameter identification of a hysteresis model of magnetostrictive actuators. Neurocomputing 70, 749–761.

Zheng, X.J., Sun, L., Jin, K., 2009. A dynamic hysteresis constitutive relation for giant magnetostrictive materials. Mech. Adv. Mater. Struct. 16, 516–521.

Zhou, H.M., Zheng, X.J., Zhou, Y.H., 2006. Active vibration control of nonlinear giant magnetostrictive actuators. Smart Mater. Struct. 15, 792–798.